Nuclear Instruments and Methods in Physics Research B 555 (2024) 165490

Contents lists available at ScienceDirect

Nuclear Inst. and Methods in Physics Research, B

journal homepage: www.elsevier.com/locate/nimb

Full Length Article

Measurement of the $^{11}B(p,\alpha_0)^8Be$ and the $^{11}B(p,\alpha_1)^8Be^*$ reactions cross-sections at the proton energies up to 2.2 MeV

Sergey Taskaev [a,b,c,*], Victor Bessmeltsev [d], Marina Bikchurina [a,b], Timofey Bykov [a,b], Dmitrii Kasatov [a,b], Iaroslav Kolesnikov [a,b], Alexey Nikolaev [e], Efim Oks [e,f], Georgii Ostreinov [a,b], Sergey Savinov [a,b], Anna Shuklina [a,b], Evgeniia Sokolova [a,b], Georgy Yushkov [e]

[a] Budker Institute of Nuclear Physics, 11 Lavrentiev ave., 630090 Novosibirsk, Russia
[b] Novosibirsk State University, 2 Pirogov str., 630090 Novosibirsk, Russia
[c] Joint Institute for Nuclear Research, 6 Joliot-Curie str., 141980 Dubna, Russia
[d] Institute of Automation and Electrometry, 1 Koptyug ave., 630090 Novosibirsk, Russia
[e] Institute of High Current Electronics, 2/3 Akademicheskii ave., 634055 Tomsk, Russia
[f] Tomsk State University of Control Systems and Radio-Electronics, 74 Vershinin str., 634034 Tomsk, Russia

ARTICLE INFO

Keywords:
Cross-section
Proton beam
Boron target

ABSTRACT

The proton boron fusion reaction attracts the attention of scientist since the dawn of nuclear physics for its relevance and potential application in different fields, from aneutronic fusion to astrophysics and hadron therapy. This reaction has been studied since the 1930s, but data from different authors differ. Obtaining the reliable experimental data on fundamental parameters (for example, direct or sequential decay, the cross-section, the energy spectrum of α-particles, the orbital angular momentum of α-particles) is still relevant. Measurements of the reactions cross-sections were carried out at the accelerator-based neutron source VITA at Budker Institute of Nuclear Physics (Novosibirsk, Russia) using an α-spectrometer. The $^{11}B(p, \alpha_0)^8Be$ and the $^{11}B(p, \alpha_1)^8Be^*$ reactions cross-sections at the proton energies up to 2.2 MeV have been measured. The obtained data are presented in tabular form.

1. Introduction

The proton boron fusion reaction is a potential candidate for the development of the so-called aneutronic fusion [1,2], the process that can help avoiding the issues related to the high neutron flux generated in the most commonly employed deuterium–tritium reaction. The proton boron fusion reaction is of interest both in nuclear astrophysics [3,4] and in nuclear reaction analysis [5]. More recently, this reaction has been proposed for the development of proton boron capture therapy [6] and for the realization of α-particles sources using high energy and high intensity lasers [7]. This reaction is written as $^{11}B(p,\alpha)\alpha\alpha$, $^{11}B(p,3\alpha)$, or $^{11}B(p, \alpha_0)^8Be$ and $^{11}B(p, \alpha_1)^8Be^*$.

The proton boron fusion reaction has been studied since the 1930s [3–5,8–38], but data from different authors differ. Obtaining the reliable experimental data on fundamental parameters (for example, direct or sequential decay, the cross-section, the energy spectrum of α-particles, the orbital angular momentum of α-particles) is still relevant.

The aim of this work is to measure the $^{11}B(p, \alpha_0)^8Be$ and the $^{11}B(p, \alpha_1)^8Be^*$ reactions cross-sections.

2. Experimental facility

The study was carried out at the accelerator-based neutron source VITA at Budker Institute of Nuclear Physics in Novosibirsk, Russia [39,40]. The layout of the experimental facility is shown in Fig. 1.

The DC vacuum insulated tandem accelerator *1* is used to generate a proton beam and to direct it to a boron target *4* through a 1 mm collimator *3*. The proton beam has the diameter of 5 mm on the surface of the boron target. The proton beam current irradiating the boron target was typically from 1 μA to 2 μA (minimum 0.7 μA, maximum 3.5 μA); its stability was 0.4 %. The proton beam energy can vary within the range of 0.1 –2.2 MeV, keeping the high-energy stability of 0.1 %.

* Corresponding author at: 11 Lavrentiev ave., 630090 Novosibirsk, Russia.
E-mail address: taskaev@inp.nsk.su (S. Taskaev).

https://doi.org/10.1016/j.nimb.2024.165490
Received 25 February 2024; Received in revised form 8 July 2024; Accepted 27 July 2024
Available online 2 August 2024

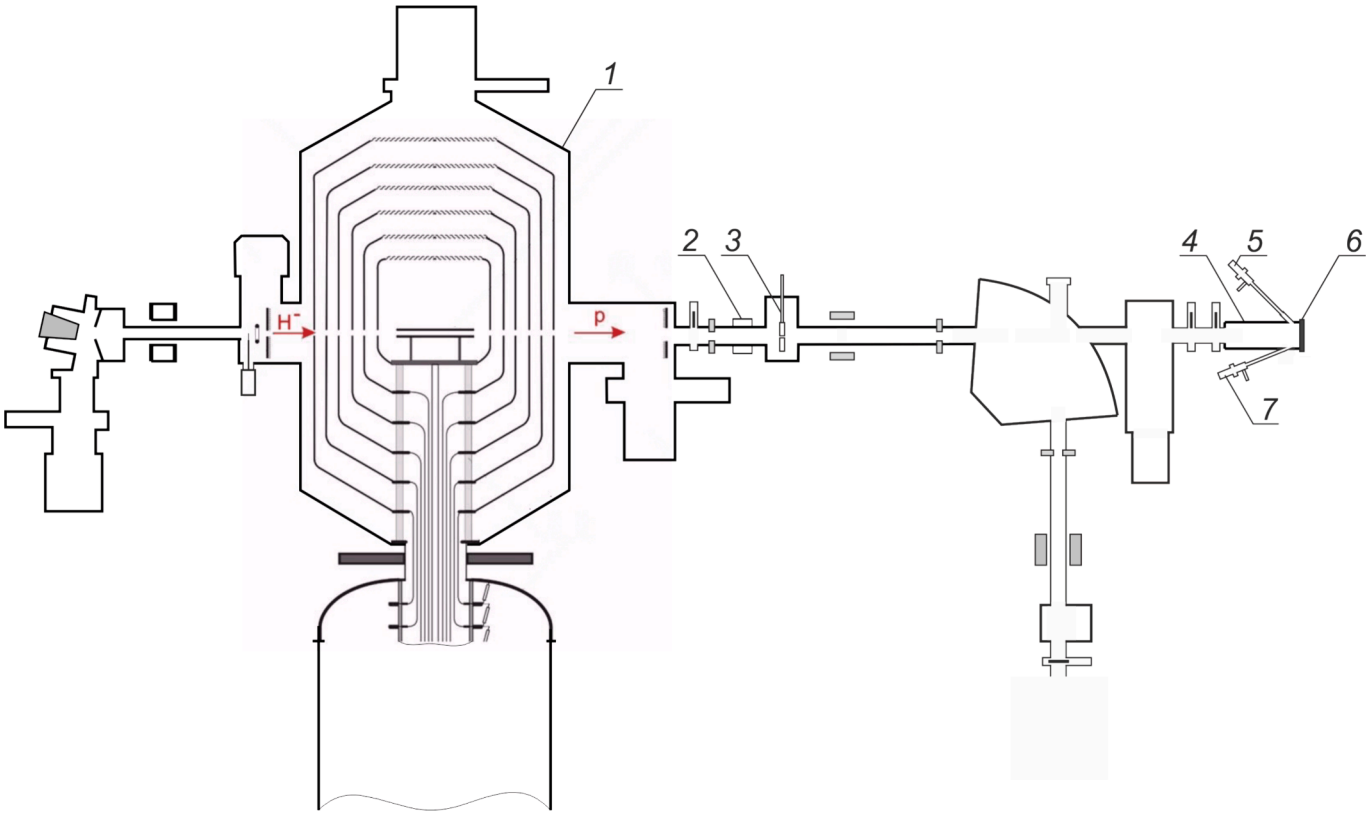

Fig. 1. Scheme of the experimental facility: *1* – vacuum insulated tandem accelerator, *2* – non-destructive DC current transformer, *3* – collimator, *4* – target assembly, 5 –α-spectrometer at 135°, 6 – boron target, *7* – α-spectrometer at 168°.

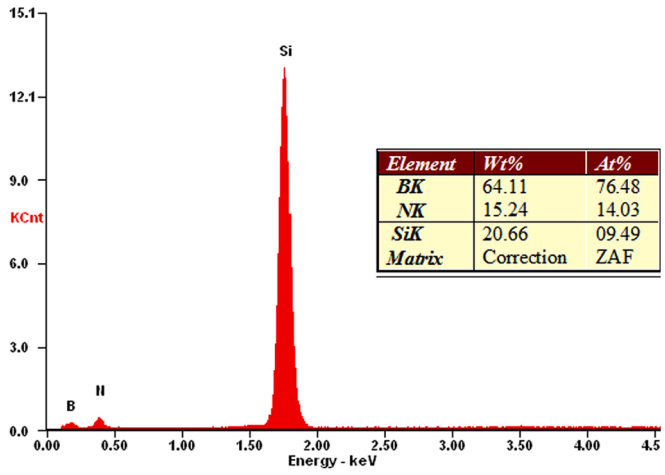

Fig. 2. Results of the composition analysis of the boron coating deposited on a KEF-25 silicon substrate of ⟨100⟩ crystal orientation, performed using the Philips SEM 515 scanning electron microscope with the EDAX ECON IV microanalyzer attachment.

The proton beam current is measured and controlled by a non-destructive DC current transformer NPCT (Bergoz Instrumentation, France) *2* [41] and by a calibrated resistance connected to the target assembly, which is electrically isolated from the facility. Although the target assembly is made in the form of a deep Faraday cup, there is electron emission from it at a level of 1 % of the ion current. Such electron emission increases the ion current by 1 %, and this fact is taken into account.

The resistive divider connected to the high-voltage electrode of the accelerator is used to measure the proton energy with the accuracy of 0.1 % [42]. The resistive divider is calibrated by the ^{7}Li(p,n)^{7}Be and the ^{9}Be(p,n)^{9}B threshold reactions.

The intensity and energy of charged particles (reaction products) were measured by the α-spectrometer (*5* and *7* in Fig. 1) with silicon semiconductor detector PDPA-1 K (Institute of Physical and Technical Problems, Dubna, Russia). Sensitive surface area of the detector is S=20 ± 1 mm^2; energy resolution – 13 keV; energy equivalent of noise – 7 keV; capacity – 30 pF; entrance window thickness – 0.08 μm; standard natural background in the range of 3–8 MeV – 0.15 imp/cm^{2}h.

The measurements were carried out with two options for placing the α-spectrometer; in Fig. 1 they are shown as *5* and *7*. At the position *5* the α-spectrometer is placed at the angle of 135° at the distance of R=717 ± 1 mm from the place of generation of charged particles from boron; at the position *7* the α-spectrometer is placed at the angle of 168° at the distance of R=707 ± 1 mm. The solid angles are $\Omega_{lab} = S/R^2 = 3.89 \times 10^{-5}$ at the angle of 135° and $\Omega_{lab} = 4.00 \times 10^{-5}$ at the angle of 168°, where S=20 ± 1 mm^2 (according to the passport data for the silicon spectrometric radiation detector; registration number 15264-96). The accuracy of the solid angle measurement is determined by the measurement error of the spectrometer detector area and is 5 %.

We consider the detection efficiency of α-particles to be equal to 100 %. The α-spectrometer was calibrated using two standard radiation sources based on the plutonium-239 radionuclide with activities of $4.01 \cdot 10^5$ Bq (passport No. 6887, marking 7165, 2P9-405.85, issue date 12.09.1985) and 1.21×10^5 Bq (passport No. 6882, marking 7160 1P9-105.85, issue date 12.09.1985). The confidence interval of each source activity measurement total error equals 19 % according to the passport. To determine the detection efficiency k of the α-spectrometer, the reference radiation sources were placed at the distance of 102.8 mm from the detector surface, and the activities were measured. The measured activities of the sources amounted to 4.16×10^5 Bq and 1.22×10^5 Bq, which is 4 % and 1.5 % higher than the passport ones; they corresponded to passport values within the margin of error. Since the

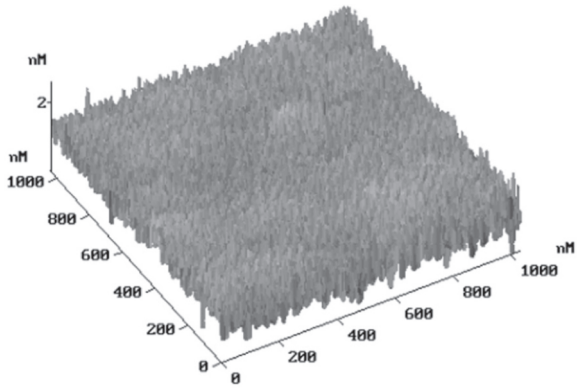

Surface: 1033.1 nm x 1043.3 nm
Peak to peak: R_{max} = 2.107 nm
Mean: R_{mean}= 1.206 nm
Roughness: R_a = 0.187 nm
Root-Mean-Sq: R_q = 0.232 nm
Skewness: R_{sk} = -0.007
Kurtosis: R_{ku} = 2.892

Fig. 3. Morphology and surface characteristics of the 1 μm thick boron coating deposited in the nitrogen environment on the silicon surface, obtained using a Solver P47 scanning atomic force microscope with an NSG-01 cantilever.

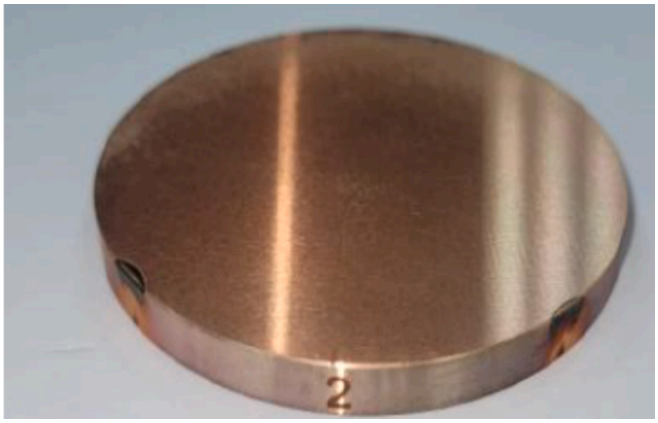

Fig. 4. Photo of the boron target: the copper substrate with 1 μm of deposited boron.

measured values of the source activity correspond to the passport ones and the reference radiation sources are independent, then the calibration confirms the assumption that the detection efficiency of α-particles can be considered equal to 100 %, i.e. k = 1.

The energy calibration of the spectrometer was carried out using the exemplary spectrometric α-source with the ^{226}Ra isotope (passport No. 425/331/10692-A, 21.10.1977) with the activity of 3.84 × 10^4 Bq, characterized by following energies of α-particles: 4748, 5453, 5966, and 7651 keV. It was established that the dependence of the energy E on a channel number N was linear and was described by the expression E [keV] = 1.3941·N+82.003.

3. Boron target

The boron target is a thin layer of boron deposited on a copper disk with the diameter of 50 mm and the thickness of 4 mm. The planar magnetron with the thermal insulated target made of pure (99.9 at. %) crystalline boron, heated in a magnetron sputtering discharge to a conductive state (about 450 °C), was used to deposit boron onto the surface of the copper substrate.

The procedure for applying boron coating to the surface of the substrate was as follows. The surface of the substrate was cleaned in an ultrasonic bath in pure distilled water at the temperature of 50 °C for 20 min. Then, after complete drying, the substrate was placed on a movable stainless steel holder of the magnetron sputtering unit. The distance from the magnetron target surface to the substrate surface was 6 cm. Previously, the vacuum chamber of the magnetron with the volume of 0.7 m^3 was pumped out by the oil-free cryogenic pump with the pumping speed of 3200 l/s to the residual pressure of 5 × 10^{-7} Torr. Then, high-purity nitrogen (99.999 vol%) was supplied to the magnetron target area with the flow rate of 0.76 l/h. The pressure in the vacuum chamber of the magnetron increased to 1 × 10^{-4} Torr, the pressure in the coating area was approximately an order of magnitude higher. This made it possible to ensure stable operation of the magnetron discharge with the flat boron target and arched magnetic field. The current of the magnetron discharge in the experiments was 100 ± 1 mA at the combustion voltage with a heated boron target of 721 ± 10 V.

The choice of nitrogen rather than inert argon as the working gas was due to the insufficient adhesion of the boron coating to the surface of the copper target in preliminary test experiments when using argon.

Before applying the coating, the substrate surface was ionically cleaned in the discharge. To do this, the negative pulse bias was applied to the substrate holder. The voltage pulses had the duration of 5 μs, the amplitude of 1 kV, and the repetition frequency of 100 kHz. The purification stage lased for 20 min. Then, the voltage pulses amplitude was reduced to the value of −50 V, close to the surface sputtering threshold, and the boron coating was applied to the substrates. The thickness of the coating was proportional to the sputtering time.

To determine the coating rate, the test coating was applied on a glass substrate. The thickness was measured using micro interferometry at 5 points on the glass substrate surface, from which the coating was removed. The average coating speed was 8.4 nm/min. Based on this value, the exposure times of the substrates during coating application were determined. It should also be noted that the density of the boron coating on the surface differs from the known density of crystalline boron (2.34 g/cm^3). As a rule, it lies in the range from 1.4 to 2.1 g/cm^3.

When coatings are applied in the nitrogen atmosphere, some of the nitrogen atoms combine with boron and can form boron nitride. The elemental composition of the coating on a silicon substrate was determined by Energy-Dispersive X-ray (EDX) spectroscopy using a scanning electron microscope Philips 515 SEM with an analyzer EDX PV-9901/22 at electron energy 30 keV (Fig. 2). Quantification of EDX spectra was carried out using the standard software package “EDAX Genesis” with ZAF matrix correction that takes into account the following three effects of the characteristic X-ray intensity when performing quantitative analysis: atomic number (Z) effect, absorption (A) effect, and fluorescence excitation (F) effect. The resulting spectrum and the composition of the target were determined using this technique; the results are shown in Fig. 2. The signal from silicon (SiK) presented in the table in Fig. 2 is the signal from the substrate itself and does not need to be taken into account. Thus, according to the data in Fig. 2, the coating mainly contains 84.5 ± 1.7 and 15.5 ± 0.3 at. % boron and nitrogen, respectively.

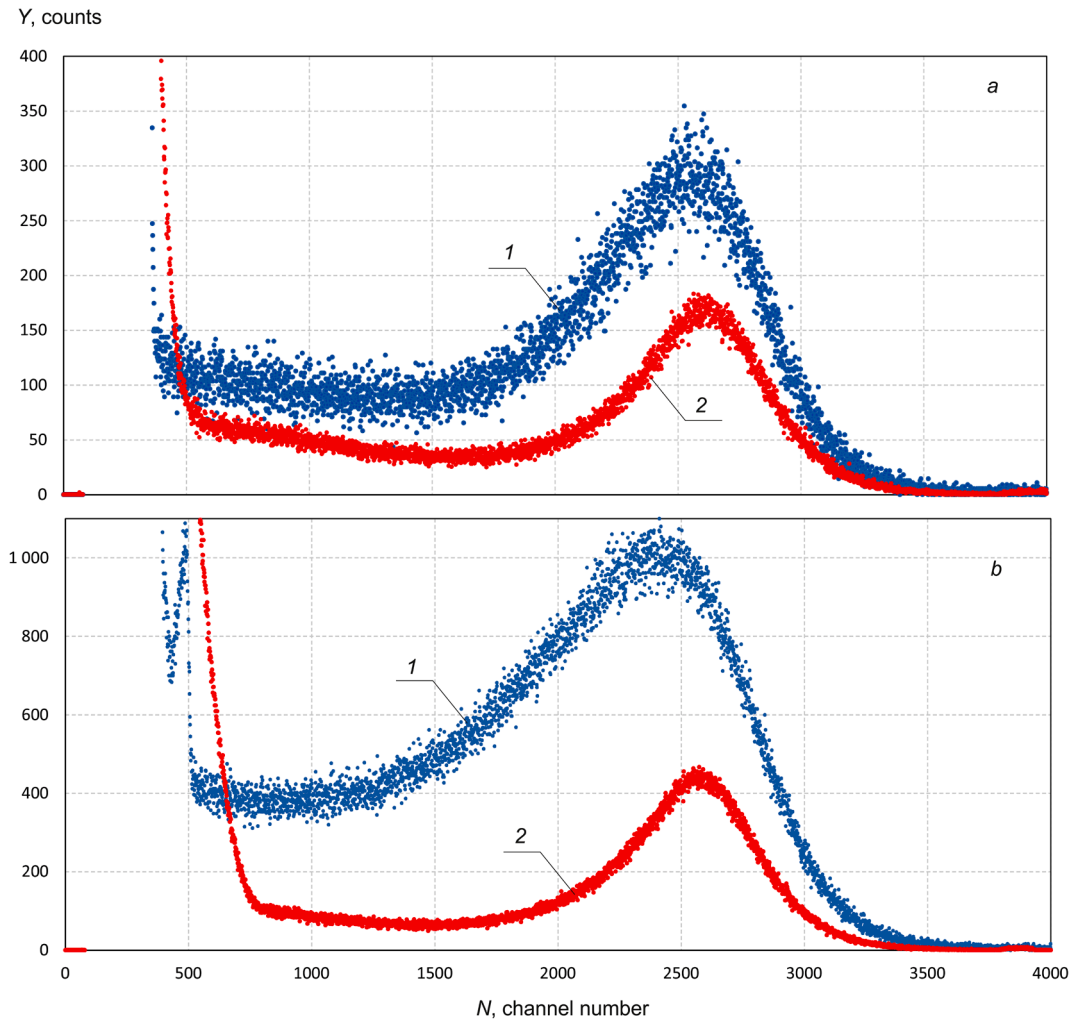

Fig. 5. The signal from the α-spectrometer at 0.5 MeV (*a*) and 0.7 MeV (*b*) proton beam: *1* – thick target, *2* – thin target.

Table 1
Coefficients A_i for boron, carbon and nitrogen.

Element	A_1	A_2	A_3	A_4
B	2.815	1206	1060	0.02855
C	2.989	1445	957.2	0.02819
N	3.35	1683	1900	0.02513

The roughness of about a micrometer thick boron films depends mainly on the roughness and properties of the substrate surface. Fig. 3 shows an example of the surface morphology of a boron coating deposited on a polished silicon substrate. From the data presented in Fig. 3 it is clear that the surface roughness of the 1 × 1 μm thick boron coating area with the thickness of 1 μm is about 0.2 nm, which is three orders of magnitude smaller than the thickness of the coating. Thus, the coating follows the surface relief of the substrate, and its surface is quite uniform at the microscopic level.

The photograph of the manufactured boron target is shown in Fig. 4. This target was pressed to the cooled substrate of the target assembly (*6* in Fig. 1) through indium-gallium paste.

The thickness of the boron was measured as follows, similar to that described in [43]. First, we measured the particle yield from a thick target then from a thin one and compared the particle yields. The thick target is one in which protons are slowed down to an energy below the particle generation reaction threshold. The thin target is one in which protons are slowed down to an energy above the particle generation reaction threshold. Knowing the dependence of the particle yield on the proton energy and measuring the particle yield from the thin and thick targets, one can determine the proton energy with which it left the layer under study and, as a consequence, determine the thickness of this layer.

The boron carbide plate B4C was used as the thick target, and the boron target was used as the thin target; the latter was then used to measure the reactions cross-sections. The measurements were carried out at the proton energies of 0.5 MeV and 0.7 MeV; the α-spectrometer was placed at the angle of 168°. The signal of the α-spectrometer normalized to the proton fluence is shown in Fig. 5. The signal to the left of 400–700 channels represents backscattered protons, the signal to the right of these channels corresponds α-particles in the ^{11}B(p, α_1)^{8}Be* reaction.

One can see that the number of detected α-particles from the thick target is greater than from the thin one: 2.10 times at the energy of 0.5 MeV and 3.95 times at the energy of 0.7 MeV.

The dependence of the proton energy loss rate S in target on its energy E is given by the expression [44]:

$$S = \frac{S_{low} \bullet S_{high}}{S_{low} + S_{high}} \text{ eV}/(10^{15} \text{ atoms/cm}^2),$$

where $S_{\text{low}} = A_1 E^{0.45}$, $S_{\text{high}} = (A_2/E) \ln[1 + (A_3/E) + (A_4E)]$, E in keV. Coefficients A_i are given in Table 1.

The proton energy loss rate in boron and carbon, determined using SRIM code [45], is in good agreement with that calculated above [44], in nitrogen it is up to 8 % lower. Despite the difference in the rate of proton loss in nitrogen, the boron thickness determined below differs by only 0.1 %, which is negligible.

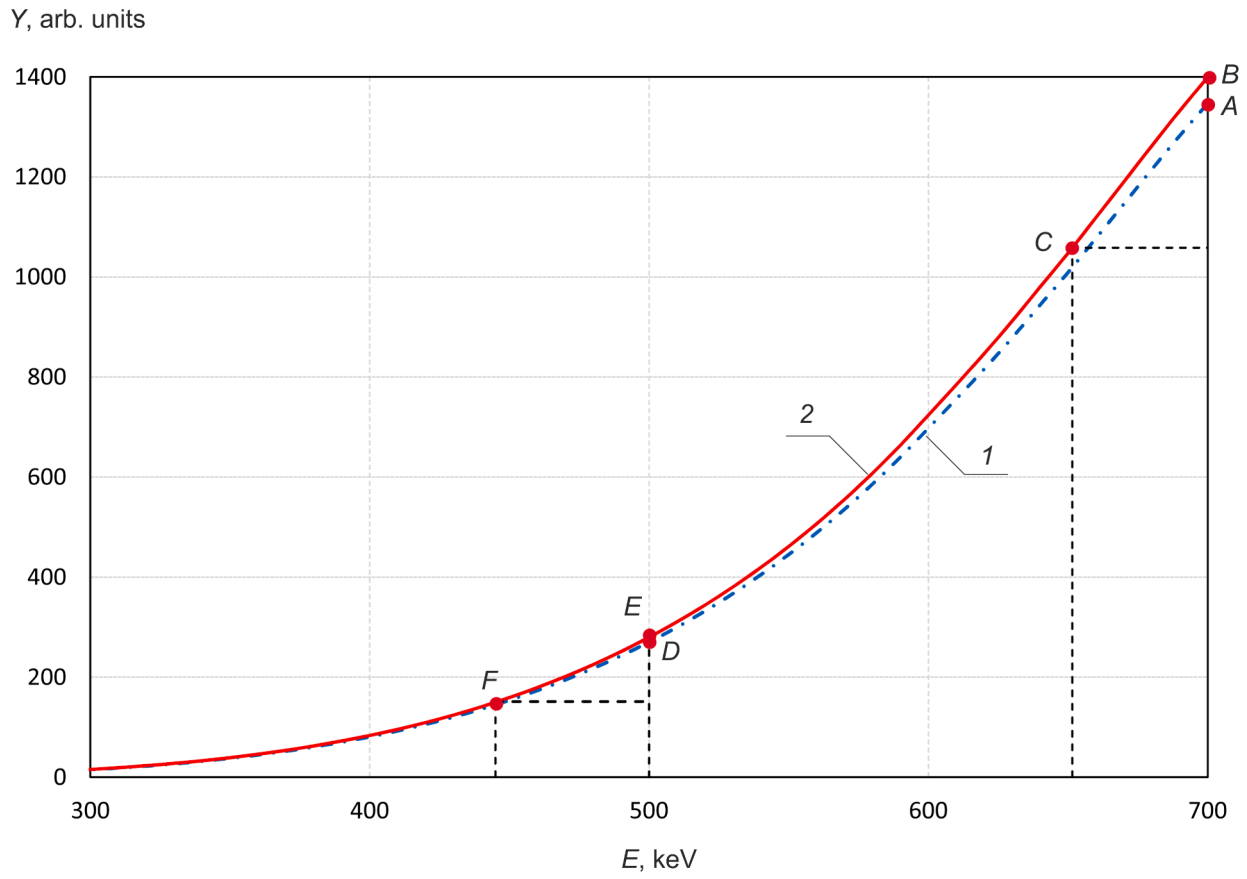

Fig. 6. The dependence of the α-particle yield *Y* on the proton energy *E* for the thick target made of boron carbide (*1*) and for the thick target made of boron with the presence of nitrogen at the concentration of 18 % (*2*).

In addition to boron, the B_4C boron carbide target contains carbon at the concentration of 20 % which for the same amount of boron increases the rate of energy loss by 29 % in the energy range 300–700 keV. The thin boron target contains nitrogen at the concentration of 18 % (see Fig. 2) which for the same amount of boron increases the rate of energy loss by 24–25 % in the same energy range.

Let us define the α-particle yield from the thick target as $Y(E)\ \int_0^E \frac{\sigma(E)}{S(E)} dE$, where σ(*E*) – the $^{11}B(p, \alpha_1)^8Be^*$ reaction cross-section, *S*(*E*) – the proton energy loss rate. Let us take the reaction cross section σ(*E*) from the article [26] and extend it to the low-energy region by dependence proportional to what we measured. Fig. 6 shows the dependence of the α-particle yield *Y* on proton energy *E* for the thick target made of boron carbide and for the thick target made of boron with the presence of nitrogen at the concentration of 18 %.

Let the yield of α-particles from the thick boron carbide target at the proton energy of 0.7 MeV to equal 1347 (point *A*) and the thick boron target to equal 1400 (point *B*). The yield of α-particles from the thin target under study is 3.95 times less than that from the thick boron carbide target, i.e. it is equal to 341. Subtract 341 from point *B* and get 1059 (point *C*). At this point *C* the proton energy is 652 keV. Knowing the proton energy loss rate in the boron target with 18 % nitrogen content one can find that the linear density of boron is equal to 9.52×10^{18} atoms/cm^2 (0.73 μm boron crystalline density).

Let us similarly determine the boron thickness at the energy of 0.5 MeV. The yield of α-particles from the thick boron carbide target to equal 270 (point *D*) and the thick boron target to equal 280 (point *E*). The yield of α-particles from the thin target under study is 2.10 times less than that from the thick boron carbide target, i.e. it is equal to 129. Subtract 129 from point *E* and get 151 (point *F*). At this point *F* the proton energy is 445 keV. Knowing the proton energy loss rate in the boron target with 18 % nitrogen content one can find that the linear density of boron is equal to 8.48×10^{18} atoms/cm^2 (0.65 μm boron crystalline density).

Additionally, the linear density of boron is determined through two more techniques.

Using the micro interferometry method it was established that the thickness of the applied layer is 1.1 μm with the accuracy of 20 %. Taking into account the boron content and its density, we obtain the linear boron thickness in the range from 6×10^{18} to 13×10^{18} atoms/cm^2.

The thickness of the applied layer was measured using the scanning electron microscope with ion column FEI Helios 650. The measured layer thickness is 1 μm with the heterogeneity of 5 %. Taking into account the boron content and its density, we obtain the linear boron thickness in the range from 7×10^{18} to 10×10^{18} atoms/cm^2.

Taking into account all measurements and uncertainties, we will assume the boron layer thickness equal to $(9.0 \pm 0.9) \times 10^{18}$ atoms/cm^2 (0.7 ± 0.07 μm boron crystalline density). We will use this boron density value when calculating the reaction cross section. The content of ^{11}B isotope is considered equal to 80.2 %.

4. Reactions

When a proton interacts with a boron nucleus, the following nuclear

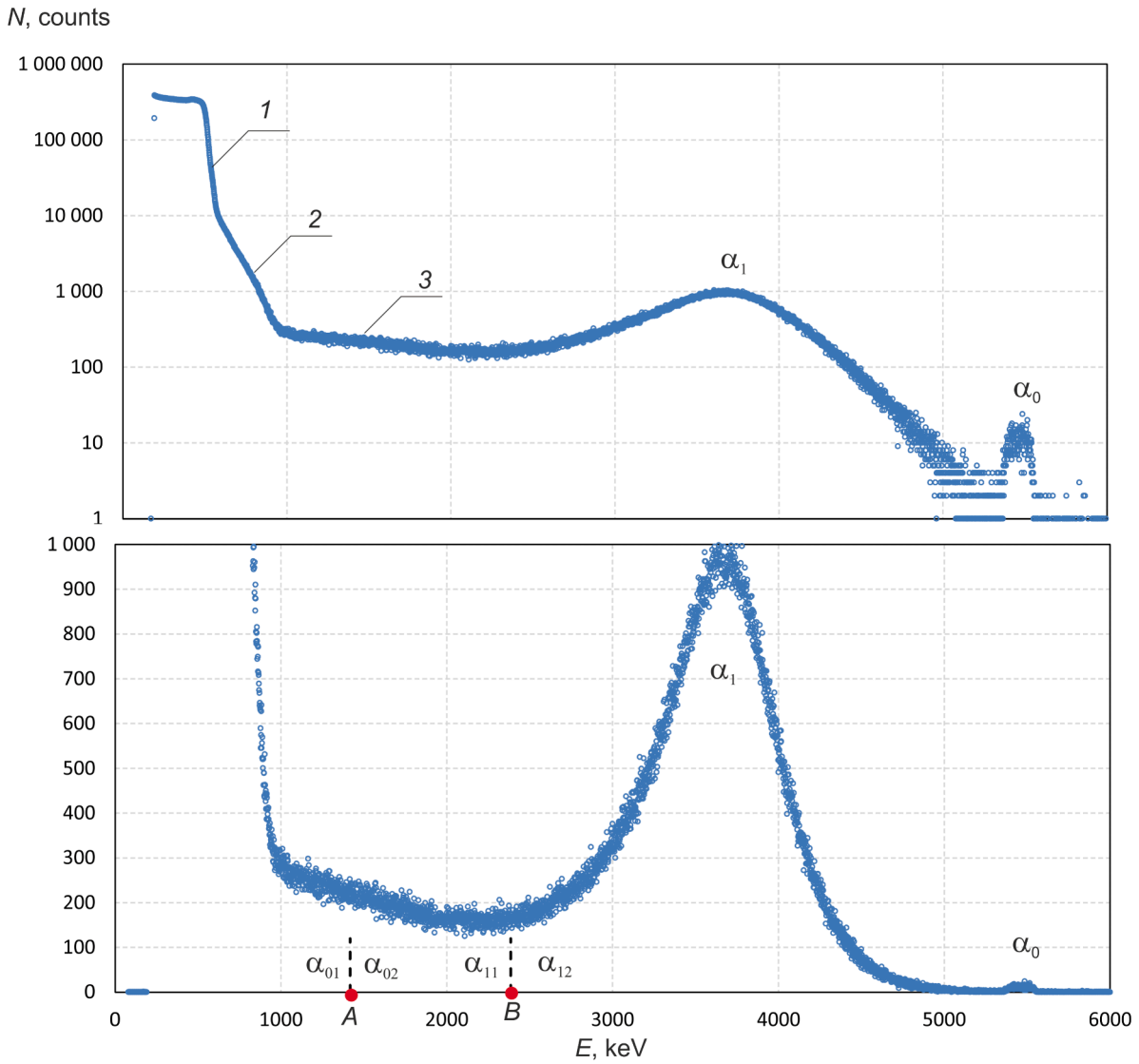

Fig. 7. The signal from the α-spectrometer at 0.6 MeV proton beam and 168°: *1* – *2* – protons backscattered on the copper substrate of the target (*1* – single events, *2* – double), *3* – α-particles.

Table 2
Measured yield of α-particles Y of the $^{11}B(p, \alpha_0)^8Be$ and the $^{11}B(p, \alpha_1)^8Be^*$ reactions at 135° and 168°: E – the average energy of the proton interacting with boron atomic nuclei, ΔE – the standard deviation of E, T_{total} – the total measurement time, T_{live} – the live time measurement by α-spectrometer, Φ – the proton flue $\alpha_0$nce.

E, keV	ΔE, keV	T_{total}, s	T_{live}, s	Φ, mC	Y, counts	
					$^{11}B(p, \alpha_0)^8Be$	$^{11}B(p, \alpha_1)^8Be^*$
135°						
75	75	3387	3377	5.81	33	1 299
134	66	2104	2079	7.20	729	15 864
247	53	2798	2759	7.34	1 608	100 431
355	45	4157	4065	7.09	3 402	350 726
461	39	3327	3174	4.28	2 832	489 685
565	35	6953	6641	5.81	4 758	1 132 297
668	32	7355	7010	6.09	6 300	1 301 732
771	29	7241	6872	5.60	5 952	693 264
873	27	7053	6701	5.20	4 908	387 033
975	25	7149	6784	5.17	4 506	276 286
1077	24	7010	6677	5.10	3 963	242 215
1178	22	7113	6787	4.99	3 282	240 986
1279	21	7106	6766	5.24	3 072	256 736
1380	20	6293	5956	5.24	2 385	251 191
1481	19	5655	5349	4.74	1 641	214 945
1582	18	7205	6849	5.52	1 533	222 377
1683	17	7206	6899	4.74	1 797	176 917
1783	17	7206	6883	5.03	2 823	172 550
1884	16	4984	4746	3.78	3 138	119 836
1985	16	7129	6814	4.92	12 753	155 504
2085	15	7207	6849	5.77	14 247	155 553
2186	14	6855	6541	5.06	6 435	135 830
168°						
75	75	6601	6571	13.83	30	3 062
134	66	15,990	15,894	35.00	3 102	47 329
247	53	11,587	11,444	39.31	5 019	340 421
355	45	4812	4737	4.67	1 464	140 414
461	39	9636	9382	9.12	3 702	623 219
565	35	7487	7205	8.16	3 936	1 045 875
668	32	7493	7210	7.59	3 885	1 011 516
771	29	10,116	9770	8.98	4 644	744 577
873	27	9527	9148	12.62	6 120	607 084
975	25	7516	7202	8.02	3 039	262 074
1077	24	6791	6493	7.70	2 385	221 382
1178	22	6807	6532	7.13	1 485	201 457
1279	21	4616	4424	4.88	747	132 521
1380	20	5954	5716	6.42	483	162 386
1481	19	6502	6234	7.13	429	211 353
1582	18	7449	7147	8.05	711	219 188
1683	17	6776	6476	7.95	747	207 286
1783	17	5636	5382	7.13	1 323	159 654
1884	16	7525	7205	9.02	6 648	193 806
1985	16	7519	7206	8.77	15 882	183 737
2085	15	3844	3697	4.24	2 355	88 345
2186	14	3193	3068	3.67	2 919	74 866

reactions occur [46]:

$^{10}B+p = \alpha + {}^7Be + 1.148$ MeV;

$^{10}B+p = \gamma + {}^{11}C + 8.693$ MeV;

$^{11}B+p = \alpha + {}^8Be + 8.588$ MeV;

$^{11}B+p = \gamma + {}^{12}C + 15.957$ MeV.

The reaction of interaction of a proton with a boron nucleus forming three α-particles can occur either via direct decay via the excited nucleus ^{12}C, or via sequential decay via the ground state of ^8Be, $^{11}B(p, \alpha_0)^8Be$, or via the first excited state, $^{11}B(p, \alpha_1)^8Be^*$:

$^{11}B+p \rightarrow {}^{12}C \rightarrow \alpha + \alpha + \alpha + 8.681$ MeV;

$^{11}B+p \rightarrow \alpha_0 + {}^8Be + 8.587$ MeV,

$^8Be \rightarrow \alpha_{01} + \alpha_{02} + 0.094$ MeV;

$^{11}B+p \rightarrow \alpha_1 + {}^8Be^* + 5.557$ MeV,

$^8Be \rightarrow \alpha_{11} + \alpha_{12} + 3.124$ MeV.

Often this reaction is written as $^{11}B(p,\alpha)\alpha\alpha$ or $^{11}B(p,3\alpha)$, but this does not mean that the reaction occurs with the simultaneous emission of three α-particles. It is believed that direct decay does not occur. We came to this opinion due to the measured energy spectrum of α-particles; spectra of direct and sequential decays differ significantly [24]. More precisely, if direct decay does occur, then its probability is much lower than the sequential decay probability; there is an estimate of the direct and the sequential decay probabilities at the end of the article.

A typical spectrum from the α-spectrometer is shown in Fig. 7.

The signal in channels below 1 MeV is due to the protons backscattered from the copper substrate of the boron target, including double events.

The sharp peak in the energy region of 5.5 MeV corresponds to primary α-particles of the $^{11}B(p, \alpha_0)^8Be$ reaction (designated as α_0). Secondary particles of this reaction, α_{01} and α_{02}, are grouped in the energy region of 1.4 MeV. On the graph, line *A* is drawn to separate these secondary particles. We can say that if one secondary particle has the energy above 1.4 MeV, then the other has a lower energy. Relative to this line, α-particles are distributed in the energy range of the order of ±0.5 MeV [28,30].

The wide peak in the energy region of 3.7 MeV corresponds to the primary α-particles of the $^{11}B(p, \alpha_1)^8Be^*$ reaction (designated as α_1). Secondary particles of this reaction, α_{11} and α_{12}, are grouped in the energy region of 2.4 MeV (line *B*). We can also say that if one secondary particle has the energy above 2.4 MeV, then the other has a lower energy. This statement is important for us to calculate the total number of α-particles in the $^{11}B(p, \alpha_1)^8Be^*$ reaction. In this reaction, two of the three α-particles have energies above 2.4 MeV (line *B*), one below. Counting the number of α-particles with energies below 2.4 MeV is difficult due to the presence of backscattered protons, secondary α-particles of the $^{11}B(p, \alpha_0)^8Be$ reaction, and α-particles of the $^{10}B(p,\alpha)^7Be$ reaction. Therefore, we will count the number of α-particles with the energy above 2.4 MeV (this energy varies slightly with the proton energy and the angle of detection) and multiply by 3/2 in order to determine the total number of α-particles in the $^{11}B(p, \alpha_1)^8Be^*$ reaction.

5. Measuring reaction cross-sections

The cross-sections of the reactions $^{11}B(p, \alpha_0)^8Be$ and $^{11}B(p, \alpha_1)^8Be^*$ were measured as follows. A thin layer of boron was irradiated with a proton beam, and the α-spectrometer measured α-particles emitted at a certain solid angle. The differential cross-section of the reaction in the laboratory coordinates dσ/dΩ was found from the formula:

$$\frac{d\sigma}{d\Omega} = \frac{eY}{Nknl\Phi\,\Omega_{lab}}$$

where e is the elementary charge, Y the experimental yield of α-particles (integrated peak counts), N the number of measured charged particles in the reaction (N=3), k the efficiency of registration of α-particles by the spectrometer ($k = 1$), nl the linear density of boron-11 nuclei ($nl = 7.2 \times 10^{18}$ cm^{-2} with the accuracy of 10 %), Φ the proton fluence (accuracy of 1 %), Ω_{lab} the solid angle ($\Omega_{lab} = 3.89 \times 10^{-5}$ at the angle of 135°; $\Omega_{lab} = 4.00 \times 10^{-5}$ at the angle of 168° with the accuracy of 5 %).

The relationship of the differential cross-section in the center of mass system $d\sigma_{c.m.}/d\Omega_{c.m.}$ and in the laboratory coordinates dσ/dΩ is given by the formula [47]:

$$\frac{d\sigma_{c.m.}}{d\Omega_{c.m.}} = \frac{|1+\beta\ cos\theta|}{(1+\beta^2+2\beta\ cos\theta)^{\frac{3}{2}}}\frac{d\sigma}{d\Omega}$$

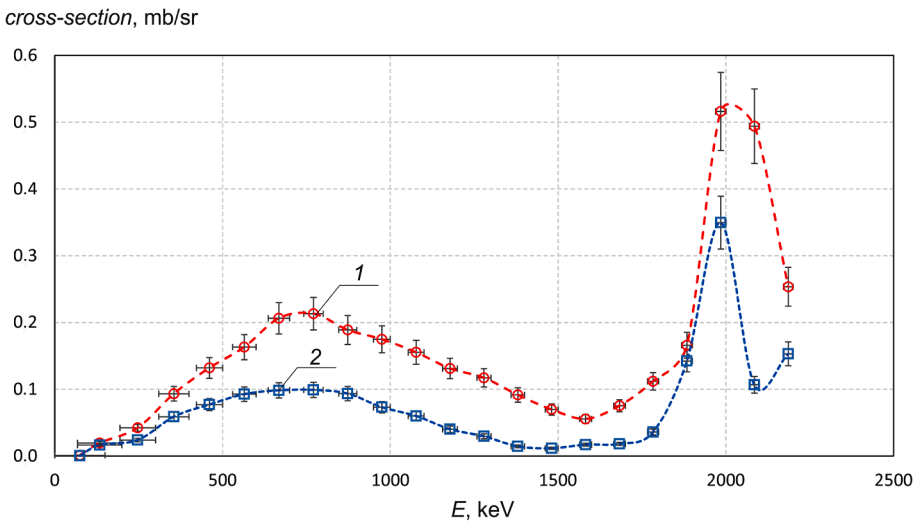

Fig. 8. The measured differential cross-section of the ^{11}B(p, α_0)^{8}Be reaction at 135° (*1*) and 168° (*2*). Differential cross-sections are in the center-of-mass system.

Table 3
The differential cross-section of the ^{11}B(p, α_0)^{8}Be reaction (in the center-of-mass system) at 135°: *E* – the proton energy, Δ*E* – the standard deviation of *E*, σ – the cross-section, Δσ – the statistical variance of σ.

E, keV	Δ*E*, keV	σ, mb/sr	Δσ, mb/sr
75	75	0.0011	0.0003
134	66	0.019	0.003
247	53	0.042	0.005
355	45	0.093	0.011
461	39	0.132	0.015
565	35	0.163	0.019
668	32	0.206	0.024
771	29	0.213	0.024
873	27	0.189	0.022
975	25	0.175	0.020
1077	24	0.155	0.018
1178	22	0.131	0.015
1279	21	0.117	0.014
1380	20	0.091	0.011
1481	19	0.070	0.008
1582	18	0.056	0.007
1683	17	0.075	0.009
1783	17	0.112	0.013
1884	16	0.166	0.019
1985	16	0.516	0.058
2085	15	0.494	0.056
2186	14	0.253	0.029

Table 4
The differential cross-section of the ^{11}B(p, α_0)^{8}Be reaction (in the center-of-mass system) at 168°: *E* – the proton energy, Δ*E* – the standard deviation of *E*, σ – the cross-section, Δσ – the statistical variance of σ.

E, keV	Δ*E*, keV	σ, mb/sr	Δσ, mb/sr
75	75	0.0004	0.0001
134	66	0.016	0.002
247	53	0.024	0.003
355	45	0.059	0.007
461	39	0.077	0.009
565	35	0.093	0.011
668	32	0.098	0.011
771	29	0.099	0.011
873	27	0.093	0.011
975	25	0.073	0.009
1077	24	0.060	0.007
1178	22	0.040	0.005
1279	21	0.030	0.004
1380	20	0.015	0.002
1481	19	0.012	0.002
1582	18	0.017	0.002
1683	17	0.018	0.002
1783	17	0.036	0.004
1884	16	0.142	0.016
1985	16	0.350	0.040
2085	15	0.107	0.013
2186	14	0.153	0.018

where $\beta = \sqrt{\frac{m_p \widetilde{M}}{M_B M} \bullet \frac{T_M}{T_M+Q}}$ and $T_M = E_p \frac{M}{(m_p+M)}$, M, $\widetilde{M}$ are the masses of the decay particles, m_p the proton mass, M_B the mass of the target particle, in this case mass of boron-11, θ the particle detection angle in the laboratory coordinates, in this case 135° or 168°, Q the reaction energy yield, E_p the kinetic energy of incident proton. For convenience we introduce the coefficient connecting the coordinate systems *G:*

$$G = \frac{|1+\beta\ cos\theta|}{(1+\beta^2+2\beta\ cos\theta)^{\frac{3}{2}}}$$

If the radiation is isotropic in the center of mass system, then the cross section of the reaction σ will be defined as: $\sigma = 4\,\pi\,G\,d\sigma/d\Omega$. If the radiation is anisotropic and is described as $\frac{d\sigma(\theta)}{d\Omega}_{c.m.} = \frac{d\sigma(90^\circ)}{d\Omega}_{c.m.}(1+A(E)\cos^2\theta)$ [24,33,48] then the cross section will be defied as $\sigma = 4\,\pi\,(1+A(E)/3)\ d\sigma/d\Omega(90^\circ)$.

The measured yields of α-particles *Y* of the ^{11}B(p, α_0)^{8}Be and the ^{11}B(p, α_1)^{8}Be* reactions at 135° and 168° are presented in Table 2. To determine the yield of α-particles in the ^{11}B(p, α_0)^{8}Be reaction the number of events in the narrow peak α_0 (see Fig. 7) was counted and this value was multiplied by 3. To determine the yield of α-particles in the ^{11}B(p, α_1)^{8}Be* reaction the number of events from line *B* (see Fig. 7) up to the narrow peak α_0 was counted and this value was multiplied by 3/2. This procedure was used up to and including proton energies of 1.4 MeV. At higher proton energies the backscattered protons events contributed to this count region. Therefore, for proton energies greater than 1.4 MeV we counted events in the channels, starting from the maximum of the distribution α_1 to the peak α_0, and multiplied the value by 2.95 ± 0.05. This coefficient was obtained by analyzing the energy spectra of α-particles with proton energies less than or equal to 1.4 MeV. The fact that this coefficient is close to 3 indicates that the energy distribution of the primary α-particle (α_1) and one of the secondary α-particles (α_{12}) are close. This allows us to determine the average energy of another secondary α-particle (α_{11}); it is about 1.3 MeV for the proton energy of 0.6 MeV (see Fig. 7). The ability to estimate the energy of the coldest particle in the ^{11}B(p, α_1)^{8}Be* reaction allows determining the energy balance for

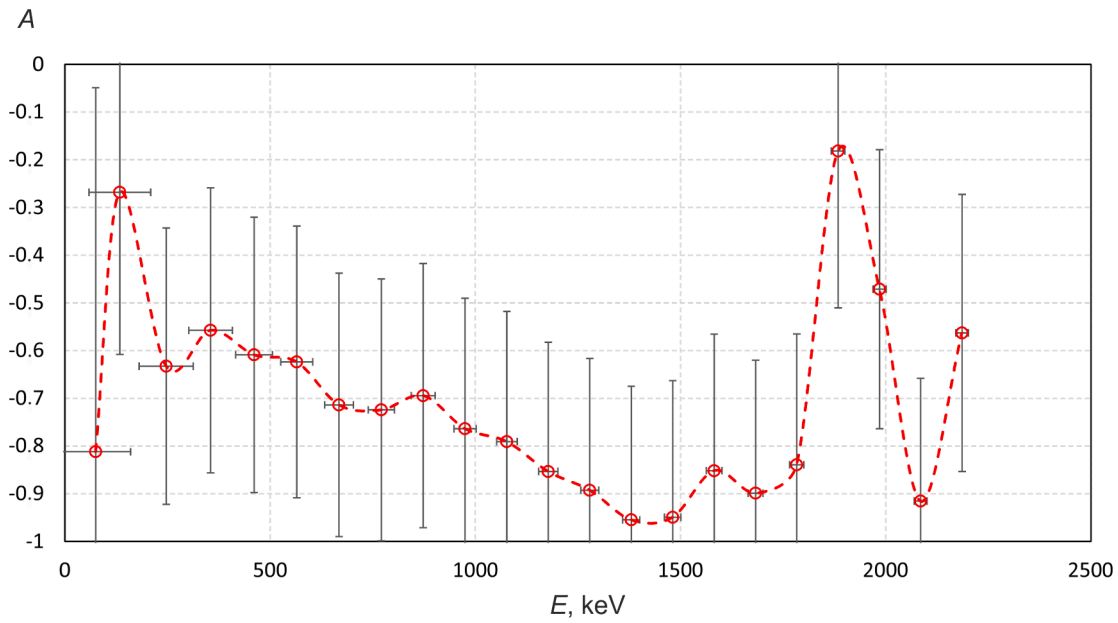

Fig. 9. The dependence of the coefficient A on the energy E.

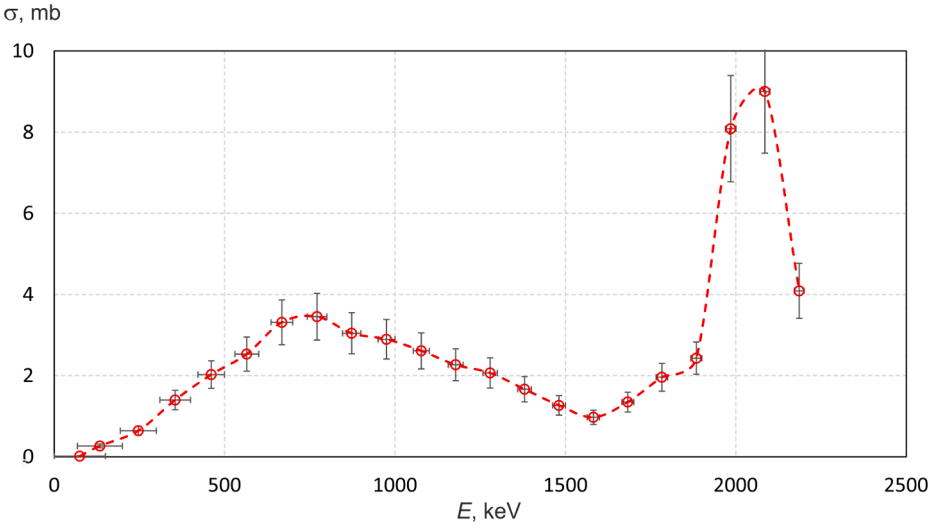

Fig. 10. The measured cross-section of the ^{11}B(p, α_0)^{8}Be reaction.

aneutronic fusion more accurately.

The measurements were carried out in 100 keV proton beam energy steps. The measured energy of the proton beam differed from the set energy by no more than 2 keV; energy stability was 1–2 keV. When a proton passes through the boron layer, the proton loses energy from 28 keV at the energy of 2.2 MeV to 150 keV at the energy of 0.15 MeV (taking into account the presence of nitrogen in the boron layer). Table 2 gives exactly this proton energy, namely the average energy in the boron layer, not the energy of the incident proton at the boron surface.

6. ^{11}B(p, α_0)^{8}Be reaction

The data obtained make it possible to determine the differential cross-section of the ^{11}B(p, α_0)^{8}Be reaction; the data are given in Fig. 8 and in Tables 3 and 4. The accuracy of the cross-section measurement is determined by the accuracy of the boron thickness determination (10 %), the accuracy of the proton fluence determination (1 %), the accuracy of the solid angle determination (5 %), and the statistical uncertainty (2–30 %); in total it is 12–33 %.

There is data here measured by other groups [5,35,37]. A comparison of these data with ours and a discussion are provided below in the discussion section.

Fig. 8 clearly shows that the radiation is anisotropic. Let it be described as $\frac{d\sigma(\theta)}{d\Omega}_{c.m.} = \frac{d\sigma(90^\circ)}{d\Omega}_{c.m.}(1 + A(E)\cos^2\theta)$. Since the measurements were carried out at two angles, we determine the coefficient $A(E)$. The dependence of the coefficient A on the energy is shown in Fig. 9.

If we integrate over all angles we get the total cross-section as a function of energy:

$$\sigma(\theta)_{c.m.} = \frac{d\sigma(90^\circ)}{d\Omega}_{c.m.} \int_0^{2\pi} d\varphi \int_0^{\pi} (1 + A(E)\cos^2\theta)\sin\theta \, d\theta = \ldots$$

Table 5
The cross-section of the ^{11}B(p, α_0)^{8}Be reaction: E – the proton energy, ΔE – the standard deviation of E, σ – the cross-section, Δσ – the statistical variance of σ.

E, keV	ΔE, keV	σ, mb	Δσ, mb
75	75	0.017	0.008
134	66	0.27	0.05
247	53	0.64	0.10
355	45	1.40	0.24
461	39	2.02	0.34
565	35	2.53	0.42
668	32	3.31	0.55
771	29	3.45	0.57
873	27	3.04	0.50
975	25	2.90	0.49
1077	24	2.61	0.44
1178	22	2.27	0.39
1279	21	2.07	0.37
1380	20	1.66	0.31
1481	19	1.27	0.24
1582	18	0.97	0.18
1683	17	1.35	0.24
1783	17	1.96	0.34
1884	16	2.43	0.40
1985	16	8.08	1.30
2085	15	9.00	1.52
2186	14	4.09	0.68

Table 6
The differential cross-section of the ^{11}B(p, α_1)^{8}Be* reaction (in the center-of-mass system) at 135°: E – the proton energy, ΔE – the standard deviation of E, σ – the cross-section, Δσ – the statistical variance of σ.

E, keV	ΔE, keV	σ, mb/sr	Δσ, mb/sr
75	75	0.04	0.005
134	66	0.42	0.048
247	53	2.64	0.30
355	45	9.62	1.08
461	39	22.8	2.5
565	35	38.8	4.4
668	32	42.6	4.8
771	29	24.8	2.8
873	27	14.9	1.7
975	25	10.7	1.2
1077	24	9.5	1.1
1178	22	9.6	1.1
1279	21	9.8	1.1
1380	20	9.6	1.1
1481	19	9.1	1.1
1582	18	8.1	0.9
1683	17	7.4	0.9
1783	17	6.8	0.8
1884	16	6.3	0.7
1985	16	6.3	0.7
2085	15	5.4	0.6
2186	14	5.3	0.6

Finally:

$$\sigma(\theta)_{c.m.} = 4\pi \frac{d\sigma(90^\circ)}{d\Omega}_{c.m.} \left(1 + \frac{A(E)}{3}\right)$$

Then we obtain the reaction cross section by integrating the yield over the angle; it is given in Fig. 10 and in Table 5.

7. ^{11}B(p, α_1)^{8}Be* reaction

The data obtained make it possible to determine the differential cross-section of the ^{11}B(p, α_1)^{8}Be* reaction; the data are given in Fig. 11 and in Tables 6 and 7. The accuracy of the cross-section measurement is determined by the accuracy of the boron thickness determination (10 %), the accuracy of the proton fluence determination (1 %), the accuracy of the solid angle determination (5 %), the accuracy of counting the number of events at energies above 1.4 MeV (3 %), and the statistical uncertainty (0.1–2 %); in total it is 12 %. There is only one measurement result for this reaction cross-section in the IBANDL database [38] (article [26]); discussion is given below in the discussion section.

Fig. 11 clearly shows that the radiation is anisotropic. Let it be described as $\frac{d\sigma(\theta)}{d\Omega}_{c.m.} = \frac{d\sigma(90^\circ)}{d\Omega}_{c.m.} (1 + A(E)\cos^2\theta)$. Since the measurements were carried out at two angles, we determine the coefficient $A(E)$. The dependence of the coefficient A on the energy is shown in Fig. 12.

Then we obtain the ^{11}B(p, α_1)^{8}Be* reaction cross-section by integrating the yield over the angle similar to what was done with the ^{11}B(p, α_0)^{8}Be reaction; the data are given in Fig. 13 and in Table 8.

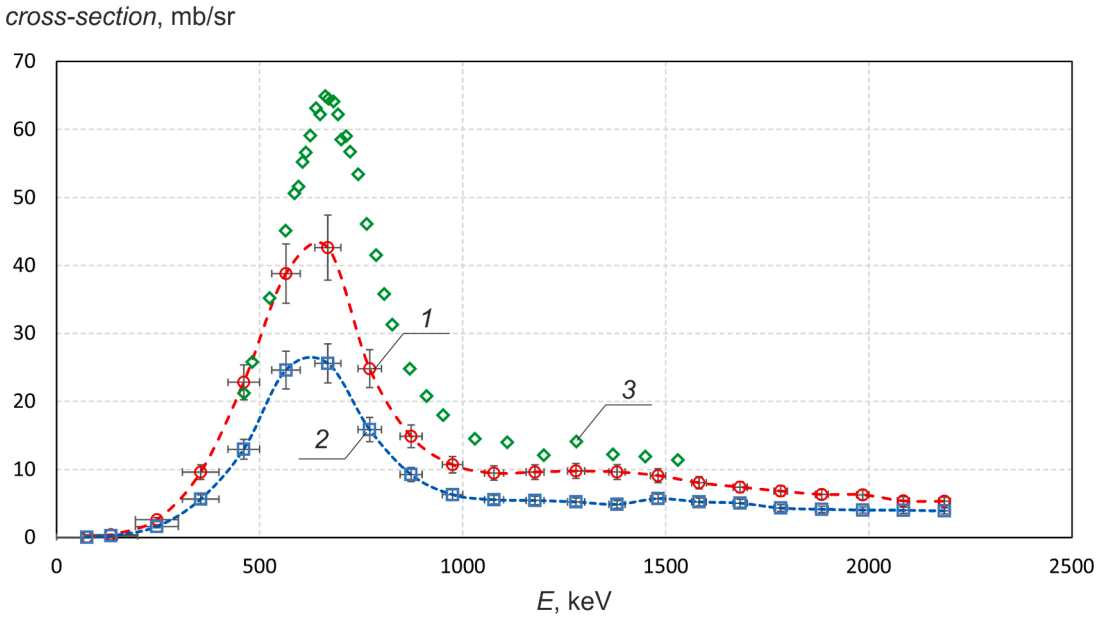

Fig. 11. The measured differential cross-section of the ^{11}B(p, α_1)^{8}Be* reaction at 135° (1) and 168° (2). Differential cross-sections are in the center-of-mass system. The reaction cross-section at 150° (3) from article [26] is also presented.

Table 7
The differential cross-section of the $^{11}B(p, \alpha_1)^8Be^*$ reaction (in the center-of-mass system) at 168°: E – the proton energy, ΔE – the standard deviation of E, σ – the cross-section, Δσ – the statistical variance of σ.

E, keV	ΔE, keV	σ, mb/sr	Δσ, mb/sr
75	75	0.04	0.005
134	66	0.25	0.03
247	53	1.62	0.18
355	45	5.65	0.63
461	39	13.0	1.4
565	35	24.6	2.8
668	32	25.6	2.9
771	29	15.9	1.8
873	27	9.3	1.0
975	25	6.3	0.7
1077	24	5.6	0.6
1178	22	5.5	0.6
1279	21	5.2	0.6
1380	20	4.9	0.5
1481	19	5.7	0.7
1582	18	5.2	0.6
1683	17	5.1	0.6
1783	17	4.3	0.5
1884	16	4.2	0.5
1985	16	4.0	0.5
2085	15	4.0	0.5
2186	14	3.9	0.5

8. $^{11}B(p,\alpha)\alpha\alpha$ reaction

Fig. 14 shows the same typical spectrum from the α-spectrometer as Fig. 7 but with a larger range in energy and a smaller range in amplitude.

The reaction can proceed via direct decay into three α-particles leading to a continuous energy distribution of the α-particles (a bell-shaped form) [24]. Extreme energy value corresponds the case when one α-particle remained at rest, and the other two α-particles flew in opposite directions with the same energy, close to 9 MeV (half energy of the excited level of $^{12}C^*$). The energy spectrum of α-particles will extend from zero energy to the energy of the order of 9 MeV. Only noise or direct decay events, but not the events of sequential decay, can cause all events to the right of 6 MeV (Fig. 14).

Let us estimate the probability of the direct decay. With the proton energy of 0.6 MeV and the angle of 168°, the number of registered α-particles with the energy from 6 to 7 MeV is 66; with the energy from 7 to 8 MeV, 51, with the energy from 8 to 9 MeV, 8; and with the energy from 9 to 10 MeV, 0; in total, 117. Let us assume that all these events are the direct decay events. This assumption is reinforced by the fact that above 9 MeV, where there should be no α-particles from the direct decay, there really are none.

We claim that we have detected 117 events in the range from 6 to 9 MeV. If we assume that the ranges from 0 to 3 MeV and from 3 to 6 MeV contain the same number of events, then the total number of α-particles will be 351. If we assume that there will be the same number of α-particles in the range from 0 to 3 MeV, and there are twice as many of them in the range from 3 to 6 MeV (a bell-shaped form), then the total number of α-particles will be 468. Let us compare these values (351 and 468) with the events of the sequential decay; they are 3,936 for α_0 and 1,045,875 for α_1, for a total of 1,049,811. We find that the direct decay probability of is 2000–3000 times less than the sequential decay probability.

9. Discussion

As noted in the introduction, the interaction of a proton with boron has constantly attracted attention, and quite a lot of articles have been published [3–5,8–37]. However, these are predominantly theoretical articles or articles on simulating the energy spectrum or angular distribution. There are few articles with the results of experimental studies, and even fewer articles with data on the reactions cross-sections presented in tabular form (there is no data on the reactions cross-sections in any evaluated database – ENDF/B, JENDL, and TENDL). Let us compare our results with the existing ones.

Let's start with the $^{11}B(p, \alpha_0)^8Be$ reaction. There is quite a lot of data on the differential cross-section of the $^{11}B(p, \alpha_0)^8Be$ reaction [5,35,37]; they are shown in Fig. 15 for angles close to those measured by us. It can be seen that the data varies greatly. Our measured reaction cross-sections agree most closely with the most recent data.

We have not found any data on the total cross-section of the $^{11}B(p, \alpha_0)^8Be$ reaction. Perhaps the cross-section we determined (Fig. 10) is the

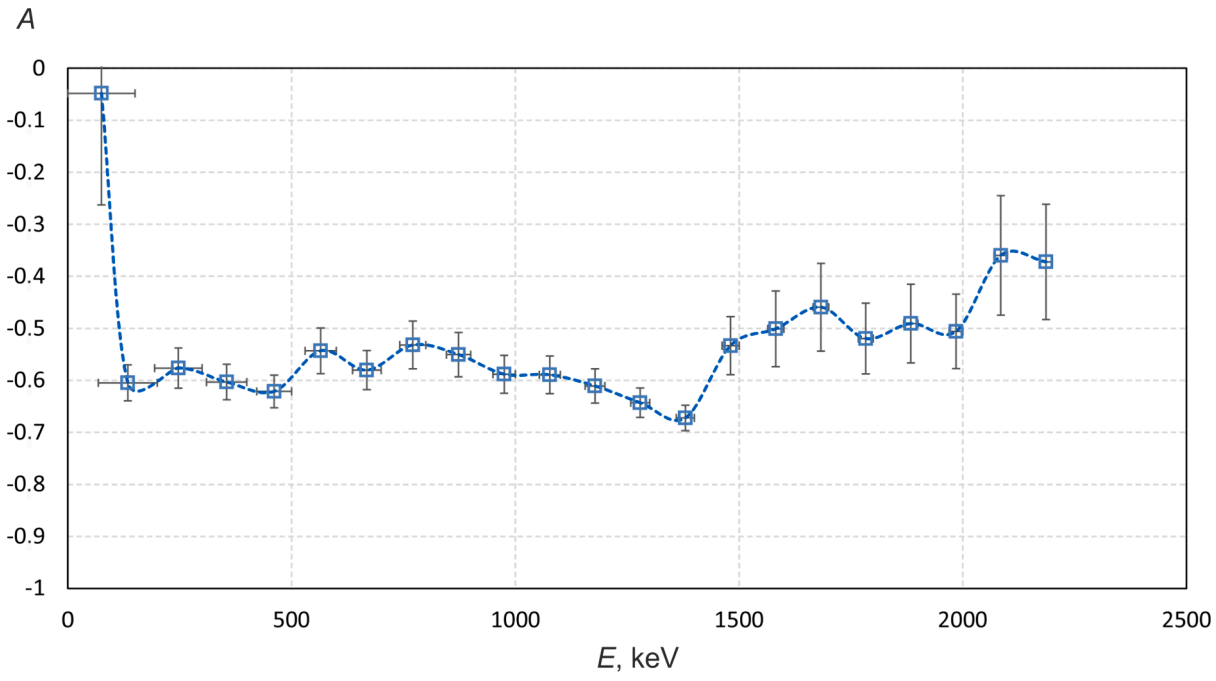

Fig. 12. The dependence of the coefficient A on the energy E.

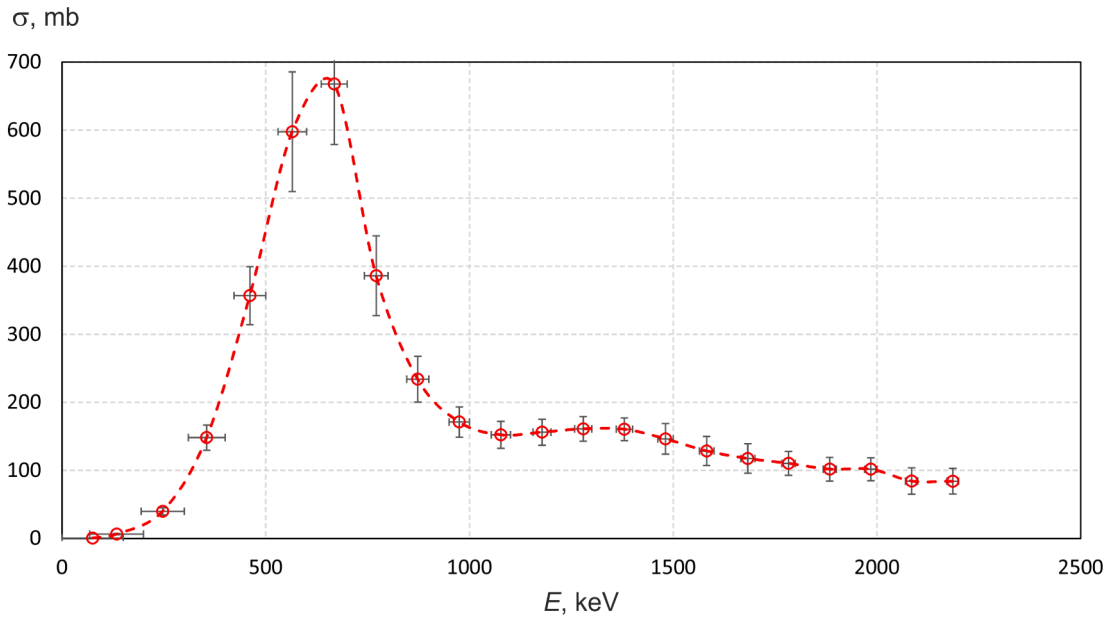

Fig. 13. The measured cross-section of the ^{11}B(p, α_1)^{8}Be* reaction.

Table 8
The cross-section of the ^{11}B(p, α_1)^{8}Be* reaction: E – the proton energy, ΔE – the standard deviation of E, σ – the cross-section, Δσ – the statistical variance of σ.

E, keV	ΔE, keV	σ, mb	Δσ, mb
75	75	0.56	0.23
134	66	6.4	0.8
247	53	40	5
355	45	148	19
461	39	357	42
565	35	598	88
668	32	668	89
771	29	386	58
873	27	234	34
975	25	171	22
1077	24	152	20
1178	22	156	19
1279	21	161	18
1380	20	160	17
1481	19	146	22
1582	18	129	21
1683	17	117	22
1783	17	110	18
1884	16	102	17
1985	16	102	17
2085	15	84	20
2186	14	84	19

first one.

There is only one measurement result of differential cross-section of the ^{11}B(p, α_1)^{8}Be* reaction cross-section [26]; it is shown in Fig. 11 compared to what we measured. It can be seen that it is equal or greater than what we measured.

There is no data on the total cross section of the ^{11}B(p, α_1)^{8}Be* reaction in the tabular form; there are only graphs in articles [30,34,37]. We will compare and analyze them. The most complete data on the total cross-section are given in [30], the dependence on energy is similar to what we measured, but the cross-section itself is 2 times larger. In the article [37], the graph shows the values at three energies, from which it can be seen that the cross-section is in good agreement with what we measured at the energy of 1 MeV, slightly higher at the energy of 1.3 MeV and 2.5 times higher than what was measured at 2 MeV. The same graph shows data with reference to the article [34] – they are in good agreement with what we measured over the entire energy range.

We have not found any experimental data on the direct decay cross-section (^{11}B(p,α)αα). Analyzing the energy spectrum of α-particles, we came to the conclusion that there is a direct decay, but its probability is much less than the sequential decay probability. We have provided an estimate of the sequential decay probability.

10. Conclusion

The proton boron fusion reaction attracts the attention of scientists since the dawn of nuclear physics for its relevance and potential application in different fields, from aneutronic fusion to astrophysics and hadron therapy. This reaction has been studied since the 1930s, but data from different authors differ.

We measured the energy spectrum of the reaction products of the proton boron interaction at proton energies up to 2.2 MeV for two angles of 135° and 168°. The shape of the energy spectrum of the reaction products indicates that the reaction with the formation of three α-particles proceeds predominantly via the ground state of ^{8}Be, ^{11}B(p, α_0)^{8}Be, or via the first excited state, ^{11}B(p, α_1)^{8}Be*. The direct decay probability is 2000–3000 times less than the sequential decay probability. The obtained data allowed us to determine the differential cross-sections of the reactions, the angular distribution of the α-particles emission, and the total reaction cross-section with high accuracy and reliability.

Funding

This work was supported by the Russian Science Foundation (grant number 19–72-30005).

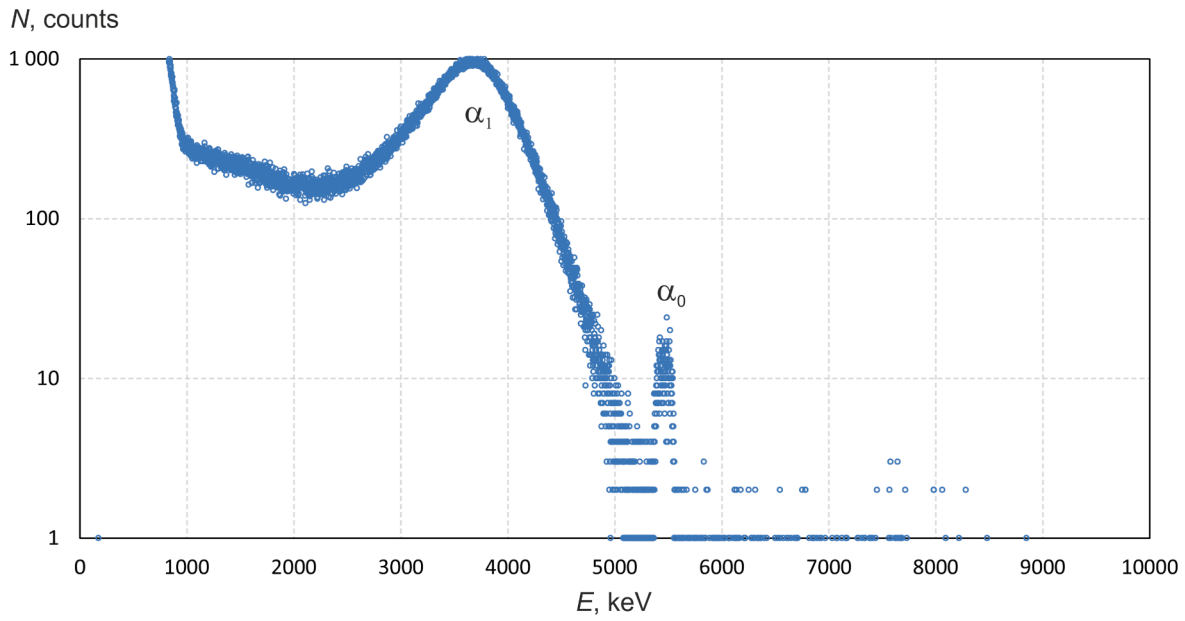

Fig. 14. The signal from the α-spectrometer at 0.6 MeV proton beam and 168°.

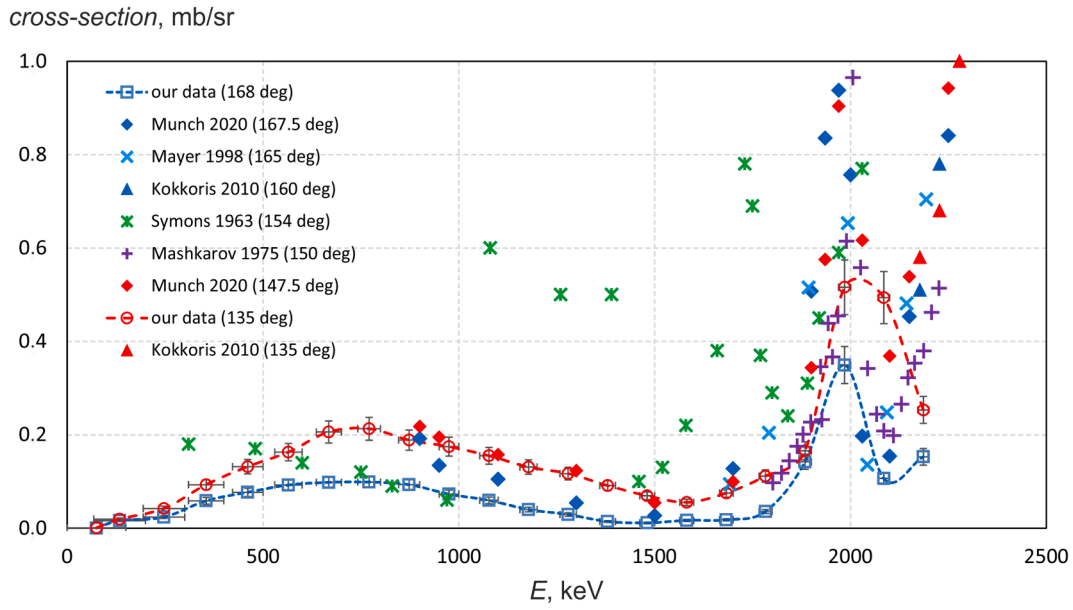

Fig. 15. Comparison of differential cross-section of the $^{11}B(p, \alpha_0)^8Be$ reaction available in the IBANDL database [38] with our measured data presented in Fig. 8.

CRediT authorship contribution statement

Sergey Taskaev: Writing – review & editing, Supervision, Conceptualization. **Victor Bessmeltsev:** Methodology, Investigation. **Marina Bikchurina:** Investigation, Data curation. **Timofey Bykov:** Visualization, Software. **Dmitrii Kasatov:** Methodology, Investigation, Data curation. **Iaroslav Kolesnikov:** Validation, Investigation. **Alexey Nikolaev:** Methodology, Investigation. **Efim Oks:** Methodology, Investigation. **Georgii Ostreinov:** Writing – original draft, Validation, Investigation. **Sergey Savinov:** Writing – review & editing, Supervision, Conceptualization. **Anna Shuklina:** Validation, Data curation. **Evgeniia Sokolova:** Validation, Methodology, Investigation, Data curation. **Georgy Yushkov:** Validation, Methodology, Investigation.

Declaration of competing interest

The authors declare that they have no known competing financial interests or personal relationships that could have appeared to influence the work reported in this paper.

Data availability

The theoretical and experimental data presented in this work are available from the corresponding authors on reasonable request.

References

[1] J.M. Dawson, Advanced fusion reactors, in: E. Teller (Ed.), Fusion, Part B, Elsevier, 1981, pp. 453–502.

[2] N. Rostoker, M. Binderbauer, H. Monkhorst, Colliding beam fusion reactor, Science 278 (5342) (1997) 1419–1422. https://doi. org/10.1126/science.278.5342.1419.

[3] L. Lamia, C. Spitaleri, V. Burjan, et al., New measurement of the $^{11}B(p,_0)^8Be$ bare-nucleus S(E) factor via the Trojan horse method, J. Phys. G Nucl. Part. Phys. 39 (2012), https://doi.org/10.1088/0954-3899/39/1/015106.

[4] Y. Yamashita, Y. Kudo, Reaction mechanism of $^{11}B(p,\alpha)^8Be$ reaction at astrophysically relevant energies, Nucl. Phys. Sect. A 589 (1995) 460–474, https://doi.org/10.1016/0375-9474(95)00069-D.

[5] M. Kokkoris, A. Kafkarkou, V. Paneta, R. Vlastou, P. Misaelides, A. Lagoyannis, Differential cross sections for the $^{11}B(p,\alpha_0)^8Be$ and $^{11}B(p,_p0)^{11}B$ reactions, suitable for ion beam analysis, Nucl. Instrum. Methods Phys. Res. Sect. B Beam Interact. Mater. Atoms 268 (2010) 3539–3545, https://doi.org/10.1016/j.nimb.2010.09.013.

[6] G.A.P. Cirrone, First experimental proof of proton boron capture therapy (PBCT) to enhance proton therapy effectiveness, Sci. Rep. 8 (2018) 1141, https://doi.org/10.1038/s41598-018-19258-5.

[7] J. Bonvalet, P. Nicolaï, D. Raffestin, et al., Energetic α-particle sources produced through proton-boron reactions by high energy high-intensity laser beams, Phys. Rev. E 103 (2021) 1–11, https://doi.org/10.1103/PhysRevE.103.053202.

[8] M. Oliphant, L. Rutherford, Experiments on the transmutation of elements by protons, Proc. r. Soc. Lond. A 141 (1933) 259, https://doi.org/10.1098/rspa.1933.0117.

[9] P.I. Dee, C.W. Gilbert, The disintegration of boron into three α-particles, Proc. r. Soc. Lond. A 154 (1936) 279–296, https://doi.org/10.1098/rspa.1936.0051.

[10] O. Beckman, T. Huus, A. Zupancic, Excitation curves for α-particles from B^{11} bombarded with protons, Phys. Rev. 91 (1953) 606, https://doi.org/10.1103/PhysRev.91.606.

[11] G. Dearnaley, G. Dissanaike, A. French, G. Lindsay Jones, Study of the B^{11}+p reaction, Phys. Rev. 108 (1957) 743–753, https://doi.org/10.1103/PhysRev.108.743.

[12] G.D. Symons, P.B. Treacy, The $B^{11}(p,\alpha)Be^8$ reaction and C^{12} states between 15 and 20 MeV, Nucl. Phys. 46 (1963) 93–107, https://doi.org/10.1016/0029-5582(63)90567-4.

[13] D. Dehnhard, D. Kamke, P. Kramer, Der Zerfall von Kohlenstoff 12 in drei α-Teilchen bei der Kernreaktion $^{11}B(p,\alpha)2\alpha$, Ann. Phys. 469 (3–4) (1964) 201–220, https://doi.org/10.1002/andp.19644690311.

[14] D. Kamke, J. Krug, F.M. Richter, Mechanism of the reaction $^{11}B(p,\alpha)2\alpha$ below and in the vicinity of the 675-keV resonance, Rev. Mod. Phys. 37 (1965) 453–454, https://doi.org/10.1103/RevModPhys.37.453.

[15] J.D. Bronson, W.D. Simpson, W.R. Jackson, G.C. Phillips, Three α-particle decay of C^{12}, Nucl. Phys. 68 (2) (1965) 241–269, https://doi.org/10.1016/0029-5582(65)90643-7.

[16] R.E. Segel, S.S. Hanna, R.G. Allas, States in C^{12} between 16.4 and 19.6 MeV, Phys. Rev. 139 (1965) B818, doi: 10.1103/PhysRev.139.B818.

[17] D. Kamke, J. Krug, Experimente zum Ablauf der Kernreaktion $^{11}B(p,3\alpha)$ in der 675 keV-Resonanz, Zeitschrift Für Phys. 201 (1967) 301–322, https://doi.org/10.1007/BF01326819.

[18] A. Giorni, D. Engelhardt, J.F. Cavaignac, J.P. Longequeue, R. Bouchez, Etude de la reaction a trois corps $11B(p,\alpha\alpha)\alpha$ de 150 keV a 2 MeV, J. Phys. 29 (1968) 4–8, https://doi.org/10.1051/jphys:019680029010400.

[19] J. Quebert, L. Marquez, Effets des résonances de ^{12}C sur l'émission de particules alpha dans la réaction $^{11}B(p,3\alpha)$, Nucl. Phys. A 126 (1969) 646–670, https://doi.org/10.1016/0375-9474(69)90854-9.

[20] Y. Chanut, J.N. Scheurer, R. Ballini, J.L. Quebert, Y. Flamant, C. Perrin, Effets des spin et parite 3^- de ^{12}C (18.36 MeV) sur la repartition des energies dans l'etat final de la reaction $^{11}B(p,3\ \alpha)$, Nucl. Phys., Sect. A 194 (3) (1972) 523–534, https://doi.org/10.1016/0375-9474(72)90999-2.

[21] P.A. Treado, J.M. Lambert, V.E. Alessi, R.J. Kane, Angular correlation and reaction mechanism for $^{11}B(p,\alpha)^8Be_{2.9}(\alpha)^4He$ with $E_p < 1.4$ MeV, Nucl. Physics, Sect. a. 198 (1) (1972) 21–32, https://doi.org/10.1016/0375-9474(72)90769-5.

[22] von W. Witsch, M. Ivanovich, D. Rendic, V. Valkovic, G. Phillips, K. Schafer, Decay of ^{12}C via the $^{11}B(p,2\alpha)\alpha$ reaction, Nucl. Phys., Sect. A 180 (2) (1972) 402–416, https://doi.org/10.1016/0375-9474(72)90869-X.

[23] J.M. Davidson, H.L. Berg, M.M. Lowry, M.R. Dwarakanath, A.J. Sierk, P. Batay-Csorba, Low energy cross sections for $^{11}B(p,3\alpha)$, Nucl. Physics, Sect. A 315 (1979) 253–268, https://doi.org/10.1016/0375-9474(79)90647-X.

[24] H.W. Becker, C. Rolfs, H.P. Trautvetter, Low-energy cross sections for $^{11}B(p,3\alpha)$, Z. Phys. A 327 (1987) 341–355, https://doi.org/10.1007/BF01284459.

[25] M. Bogovac, S. Fazinic, M. Jaksic, M. Lattuada, D. Miljanic, N. Soic, C. Spitaleri, M. Zadro, $^{11}B(p,\alpha\alpha)^4He$ reaction in collinearity configurations, Fiz. B 4 (1995) 229–236. https://hrcak.srce.hr/file/437559.

[26] J. Liu, X. Lu, X. Wang, W. Chu, Cross-sections of $^{11}B(p,\alpha)^8Be$ reaction for boron analysis, Nucl. Instrum. Methods Phys. Res. Sect. B 190 (2002) 107–111, https://doi.org/10.1016/S0168-583X(01)01272-1.

[27] V.F. Dmitriev, α-particle spectrum in the reaction $p + {}^{11}B \rightarrow \alpha + {}^8Be^* \rightarrow 3\ \alpha$, 2008, https://arxiv.org/pdf/0812.2538.pdf.

[28] S. Stave, M.W. Ahmed, R.H. France, S.S. Henshaw, B. Müller, B. Perdue, R. Prior, M. Spraker, H. Weller, Understanding the $B11(p,\alpha)\alpha\alpha$ reaction at the 0.675 MeV resonance, Phys. Lett. Sect. B Nucl. Elem. Part. High-Energy Phys. 696 (2011) 26–29, https://doi.org/10.1016/j.physletb.2010.12.015.

[29] M.C. Spraker, M.W. Ahmed, M.A. Blackston, N. Brown, R.H. France, S.S. Henshaw, B.A. Perdue, R.M. Prior, P.N. Seo, S. Stave, H.R. Weller, The $11B(p,\alpha)8Be \rightarrow \alpha + \alpha$ and the $11B(\alpha,\ \alpha)11B$ reactions at energies below 5.4 MeV, J. Fusion Energy 31 (2012) 357–367, https://doi.org/10.1007/s10894-011-9473-5.

[30] M.H. Sikora, H.R. Weller, A new evaluation of the $11B(p,\alpha)\alpha\alpha$ reaction rates, J. Fusion Energy 35 (2016) 538–543, https://doi.org/10.1007/s10894-016-0069-y.

[31] K.L. Laursen, H. Fynbo, O. Kirsebom, R. Madsboll, K. Riisager, Complete kinematical study of the 3α breakup of the 16.11 MeV state in ^{12}C, Eur. Phys. J. A 52 (2016) 271, doi: 10.1140/epja/i2016-16271-2.

[32] J.H. Kelley, J.E. Purcell, C.G. Sheu, Energy levels of light nuclei A = 12, Nucl. Phys. 968 (2017) 71–253, https://doi.org/10.1016/j.nuclphysa.2017.07.015, 71-253.

[33] M. Munch, H. Uldall Fynbo, The partial widths of the 16.1 MeV 2^+ resonance in ^{12}C, Eur. Phys. J. A 54 (2018) 1–8, https://doi.org/10.1140/epja/i2018-12577-3.

[34] F.A. Geser, M. Valente, Analytical approach to the reaction cross section of the fusion of protons with boron isotopes aimed at cancer therapy, Appl. Radiat. Isot. 151 (2019) 96–101, https://doi.org/10.1016/j.apradiso.2019.04.034.

[35] M. Munch, O.S. Kirsebom, J.A. Swartz, H.O.U. Fynbo, Resolving the $^{11}B(p,\alpha)$ cross-section discrepancies between 0.5 and 3.5 MeV, Eur. Phys. J. A 56 (2020) 1–7, https://doi.org/10.1140/epja/s10050-019-00016-8.

[36] M. Kuhlwein, K. Lytje, H. Fynbo, A. Gad, E. Jensen, O. Kirsebom, M. Munch, J. Refsgaard, K. Riisager, Exclusive decay study of the 16.62 MeV (2^-, T=1) resonance in ^{12}C, Phys. Lett. B 825 136857 (2022), https://doi.org/10.1016/j.physletb.2021.136857.

[37] D. Mazzucconi, D. Vavassori*, D. Dellasega, F.M. Airaghi, S. Agosteo, M. Passoni, A. Pola, D. Bortot, Proton boron fusion reaction: A novel experimental strategy for cross section investigation, Radiation Physics and Chemistry 204 (2023) 110727, https://doi.org/10.1016/j.radphyschem.2022.110727.

[38] https://www-nds.iaea.org/exfor/ibandl.htm.

[39] S. Taskaev, E. Berendeev, M. Bikchurina, T. Bykov, D. Kasatov, I. Kolesnikov, A. Koshkarev, A. Makarov, G. Ostreinov, V. Porosev, S. Savinov, I. Shchudlo, E. Sokolova, I. Sorokin, T. Sycheva, G. Verkhovod, Neutron source based on vacuum insulated tandem accelerator and lithium target, Biology 10 (2021) 350, https://doi.org/10.3390/biology10050350.

[40] S. Taskaev, Accelerator-based Neutron Source VITA, FizMatLit, Moscow, 2024.

[41] https://www.bergoz.com/products/npct/.

[42] M. Bikchurina, T. Bykov, D. Kasatov, Ia. Kolesnikov, A. Makarov, I. Shchudlo, E. Sokolova, S. Taskaev, The measurement of the neutron yield of the $^7Li(p,n)^7Be$ reaction in lithium targets, Biology 10 (2021) 824, doi: 10.3390/biology10090824.

[43] D. Kasatov, Ia. Kolesnikov, A. Koshkarev, A. Makarov, E. Sokolova, I. Shchudlo, S. Taskaev, Method for in situ measuring the thickness of a lithium layer, J. Instrum. 15 (2020) P10006, https://doi.org/10.1088/1748-0221/15/10/P10006.

[44] H. Andersen, J. Ziegler, Hydrogen Stopping Powers and Ranges in All Elements, Pergamon Press Inc., 1977.

[45] J.F. Ziegler, J.P. Biersack, M. Ziegler, D.J. Marwick, G.A. Cuomo, SRIM-2013 Code, IBM Company, 2013.

[46] Tables of Physical Constants, Handbook. I.K. Kikoin Edition, AtomIzdat, Moscow, 1976.

[47] Yu. Shirokov, N. Yudin, Nuclear Physics, MIR Publishers, Moscow, 1982 vols. 1 and 2.

[48] R. Resnick, D.R. Inglis, Theory of the lithium TWO-ALPHA REACtions. II. Angular distribution of $Li^6(d,\alpha)\alpha\alpha$, Phys. Rev. 76 (1949) 1318–1323, https://doi.org/10.1103/PhysRev.76.1318.